JOINT INSTITUTE FOR AERONAUTICS AND ACOUSTICS

NASA-CR-177321
19850004553

National Aeronautics and
Space Administration

Ames Research Center

Stanford University

JIAA-TR 57

VISCOUS-INVISCID AERODYNAMIC ANALYSIS OF TWO-DIMENSIONAL THRUST AUGMENTORS

Domingo A. Tavella and Leonard Roberts

STANFORD UNIVERSITY
Department of Aeronautics and Astronautics
Stanford, California 94305

SEPTEMBER 1984

JIAA-TR 57

VISCOUS-INVISCID AERODYNAMIC ANALYSIS OF TWO-DIMENSIONAL THRUST AUGMENTORS

Domingo A. Tavella and Leonard Roberts

STANFORD UNIVERSITY
Department of Aeronautics and Astronautics
Stanford, California 94305

SEPTEMBER 1984

ABSTRACT

A theory for the computation of two-dimensional thrust augmentor performance is developed. The flow field is assumed to be incompressible, of uniform density and statistically steady. The flow in and around the augmentor is assumed to consist of an outer, inviscid part and an inner, viscous part. The outer field is calculated analytically and then matched with the inner, viscous field, which is computed by means of integral methods. This form of analysis leads to a simple and economical approach, particularly useful for conducting parametric studies. The theoretical results are compared with recently acquired experimental data.

ACKNOWLEDGEMENTS

This work was supported by NASA grant NCC 2-150.

TABLE OF CONTENTS

NOMENCLATURE

a_{ij}, b_i	elements in matrix and right hand side of reduced equations
b	characteristic width of turbulent region
εt	outer edge of turbulent plane
εf_i	shroud perturbation in physical plane
h	shroud inner half width
l	shroud length
k	eddy viscocity scaling constant
K	similarity parameter
m_j	primary jet momentum
p	pressure
q_p	primary jet sink intensity
T	shroud-associated thrust
u, v	x, y velocity components
u_b	Borda velocity
u_o	outer limit of viscous solution
u_1	maximum of excess velocity in viscous region
$\hat{u}$	approximation to viscous solution
V	complex velocity
z, w	complex coordinates in physical, transformed plane
x, y	coordinates in viscous solution
x_j, ξ_j	virtual origin in physical, transformed plane
$x^* \xi^*$	wedge length in physical, transformed plane
α	ln 0.5
β	diffuser angle
δ	wedge angle in augmentcr shroud

φ	thrust augmentation
ϕ, ϕ_b, ϕ_p	velocity potential of outer flow, channel flow, primary jet entrainment
ν_t	eddy viscocity
Ω	y-projection of diffuser inner surface
ρ	density
ψ	stream function
τ	Reynolds stress in 2-d boundary layer approximation
$(\sim)$	indicates that the function is evaluated in the transformed plane
$(\cdot)$	indicates the derivative of the function with respect to its argument

INTRODUCTION

A thrust augmentor is a device where a high-momentum primary jet undergoes turbulent mixing with a secondary stream inside a shroud. The resulting thrust produced by the jet shroud combination is higher than the thrust that would result from the jet discharging in isolation. This augmentation of thrust arises from the induced pressure distribution on the surface of the shroud and from the fact that the primary jet discharges in an atmosphere at lower pressure.

In this work, effort is focused on two-dimensional augmentors with incompressible, statistically steady flow which, in view of their applications, are of particular interest. Considerable amount of work has been devoted in resent years to the development of theories to predict augmentor performance. Most of these theories fall in either of the following two categories: Those that make use of conservation laws in global form, the so-called control volume approaches, and those that actually attempt to resolve the two-dimensionality of the problem. This second category includes approaches based on the direct numerical solution of the conservation equations by finite differences or finite elements, and those that based on integral methods.

An essential element in augmentor flow analysis is the viscous-inviscid interaction taking place between the turbulent primary flow and the turbulence-free secondary flow in regions where the mixing has not extended all across the shroud cross section. In earlier theories this interaction was considerably simplified by assuming that the still unmixed secondary flow was essentially uniform, the pressure being constant on any cross section of the shroud[1,2]. This assumption is acceptable in the case of elongated jet pumps where the primary nozzle is located well inside the shroud where the secondary flow can justifiably be considered uniform. In the case of ejectors for aeronautical applications however, the primary nozzle may be located outside the shroud or close enough to the inlet so that the inviscid flow drawn into the device can by no means be considered uniform. In a more recent approach Bevilaqua et al [3,4] formulated a theory where such an interaction is taken

into account, using panel methods to compute the inviscid flow field and finite differences for the turbulent jet mixing. In the work reported here an inviscid potential outer flow and a viscous, inner flow are also distinguished. The outer flow is computed analytically using a perturbation approach around a straight-walled augmentor, and the inner flow is computed with an integral method. A matching of first order between the two flows is then performed. This combination of analysis and integral methods makes for a very economical scheme quite suitable for parametric analysis, where a large number of performance evaluations is needed.

Some of the results are compared with the measurements obtained by Bernal and Sorahia[5] at the Jet Propulsion Laboratory in Pasadena.

2. VISCOUS-INVISCID AERODYNAMIC INTERACTION

2.1 Model for the physical problem

For the sake of analysis, the flow field of a typical two-dimensional ejector will be divided in five regions, as shown in figure 1.

Region 1 will be significant when the primary nozzle is located ahead of the inlet. In such a case the primary jet develops under the influence of an inviscid flow that surrounds it, called secondary flow. The nature of this secondary flow will be affected by the shape of the inlet, the suction into the inlet and the entrainment of the primary jet. The growth characteristics of the primary jet are intimately connected with the surrounding velocity field, giving rise to a strong viscous-inviscid interaction.

Region 2 is qualitatively similar to region 1. However, the presence of solid walls allows for the introduction of the equation of conservation of mass in a simple integral form. This fact has an effect in the transition to region 3.

In region 3 the turbulent primary jet continues to develop under the influence of a surrounding potential flow. The main difference between this region and the previous two regions is that here the potential flow can be considered quasi one-dimensional. Under this assumption a simultaneous solution for both the viscous and inviscid flows is possible. In some cases recirculation may exist in this region. Although the methodology described in this work can in principle indicate the precise of recirculation, this has not been observed in the computations carried out for a practical configuration. In the absence of recirculation the turbulent part of the flow reaches the walls of the ejector towards the end of region 3.

In region 4 the flow field is turbulent all across the channel, and the pressure increases gradually downstream due to momentum dissipation. The pressure reaches atmospheric value at the end of region 4.

Region 5 constitutes the exhaust plume. Here the jet exhaust develops as a free turbulent jet and its entrainment contributes to the potential flow field surrounding the

device.

2.2 Mathematical model

A mathematical model for the problem shown in figure 1 should reflect the strong interaction taking place between the turbulent primary jet and the potential flow surrounding it and entering into the augmentor. To this end an external, inviscid solution will be computed and then matched with an internal, viscous solution. The external solution can be computed using any of the techniques available for potential flows, in the particular examples analyzed here conformal mapping and a perturbation approach will be used. The inner solution will be computed using an integral method. The internal-external matching will take place in regions 1 and 2. In regions 3 and 4 the internal flow will be computed using integral techniques developed previously[6]. The presence of wall boundary layers will be ignored. This amounts to the assumption that mass displacements by boundary layers are not too reevant in the scope of this analysis and that the change of mementum in the boundary layer is small compared with the global change of momentum in the main turbulent flow. Theoretical and experimental studies of the jet pumps[7] seem to bear out this hypothesis.

Figure 2 shows schematically the outer and inner solutions. The outer field is indicated by its streamlines, while the inner field is indicated by its velocity profiles. To facilitate the derivation of this formulation, an ejector whose shroud consists of two parallel flat plates will be considered first. Using a perturbation approach the method will then be generalized to include arbitrary shapes slightly departing from flat plates.

2.3 The straight-walled augmentor

In this case the ejector reduces to a confining channel consisting of two flat plates. The external inviscid flow field can be thought of as consisting of the superposition of three different fields, as illustrated in figure 3, where in all cases the domain of the flow is external to the shaded region. Figure 3a represents the effect of potential flow going into

the inlet. This component of the flow will be referred to as the 'Borda component', due to its similarity with the Borda mouthpiece flow field, as will be explained later. Figure 3b represents the flow due to entrainment into the primary jet and into the exhaust plume. The primary jet entrainment is represented by a distribution of singularities on the axis of symmetry. The flow field induced by the exhaust plume is not expected to affect the performance of the augmentor significantly, and will not be included in the theory.

2.3.1 The inlet suction field

This is the field shown in figure 3a. It will be assumed that it can be approximated well by the so-called Borda mouthpiece flow. This is the flow field produced by suction into a semi-infinite channel made up of parallel walls and such that the flow inside the channel becomes uniform infinitely far downstream. According to both the Borda mouthpiece solution and flow field measurements in parallel wall augmentors, the velocity distribution of the inviscid part of the flow inside the shroud becomes almost uniform within a short distance from the inlet. The adoption of the Borda mouthpiece solution also has the advantage that it can be used as a basic solution in a perturbation approach to deal with inlets of rather general shape. The flow field of the Borda mouthpiece can be found using conformal mapping. Define the complex velocity potential such that:

$$V = \frac{d\phi}{dz} \tag{2.1}$$

If a mapping $z = f(w)$ can be found where the potential is known, 2.1 can be expressed

$$V = \frac{d\tilde{\phi}}{dw}\frac{dw}{dz} \tag{2.2}$$

In our case we will identify z with the physical plane and w with a transformed plane, where the complex velocity potential can be calculated immediately. Due to symmetry, we will consider only half of the channel, as seen in figure 4. Using the Schwartz-Christofeln theorem, the shaded region in the z plane can be mapped conformally onto the upper half

of the w plane. The upper half of the z plane can be considered the exterior of a degenerate triangle of sides 1-2, 2-3, 3-1. The Schwartz-Christofeln theorem gives the transformation in integral form for the exterior of a polygon on the upper half of the w plane:

$$w = c_1 \int \Pi_{j=1}^{n} (w - w_j)^{\frac{\alpha j}{\pi} - 1} \, dw + c_2 \tag{2.3}$$

where c_1, c_2 are complex constants, w_j are the locations of the transformed positions of the vertices of the polygon, numbered in counterclockwise sense, and α_j are the internal angles at such vertices. At most three w_j's can be specified. If a vertex transforms to a point at infinity, its corresponding term will be absent from the product in 2.3. applying 2.3 to the degenerate triangle of figure 4 we have

$$z = c_1 \int \frac{w - 1}{w} dw + c_2 \tag{2.4}$$

Then the transformation is

$$z = c_1 (w - \ln w + c_3) \tag{2.5}$$

Proper orientation and scaling requires $c_1 = \frac{1}{\pi}$; $c_3 = i\pi - 1$, then

$$z = \frac{1}{\pi}(w - \ln w + i\pi - 1) \tag{2.6}$$

The logarithm in 2.6 has a phase angle in the range$-\pi < \theta < \pi$. To compute the velocity potential in the w plane, we consider the value of the potential infinitely far downstream in the z plane:

$$\phi_b \rightarrow u_b \, z \quad \text{for} \quad \bar{x} \rightarrow \infty; \; 0 < \bar{y} < 1 \tag{2.7}$$

where u_b will be called "Borda velocity". The corresponding point in the w plane is the origin. In the vicinity of $w = 0$ we can neglect w in 2.6 to get:

$$\tilde{\phi}_b = -\frac{u_b}{\pi} \ln w \tag{2.8}$$

This means that in the transformed plane the velocity potential is the one produced by a sink at the origin of intensity $2u_b$. The complex velocity of the Borda mouthpiece in the z plane is then given by:

$$V_b = -\frac{u_b}{\pi}\frac{1}{w(z)-1} \tag{2.9}$$

2.3.2 Flow induced by primary jet entrainment

To estimate the effect of the primary jet entrainment on the potential flow, consider a turbulent jet developing in an arbitrary inviscid field. The outer edge of the turbulent jet is described by the function $\epsilon t(x)$, whose magnitude will be assumed small compared with any characteristic length of the inviscid flow, $t(x)$ being a function of order 1. Now lets assume that the inviscid flow is described by a stream function defined as follows:

$$d\psi = udy - vdx \tag{2.10}$$

Then the governing differential equation and the boundary conditions for the inviscid flow field are:

$$\begin{aligned} \nabla^2\psi &= 0 \\ \psi(x,\infty) &= \psi_\infty \\ \psi(x,\epsilon t(x)) &= \epsilon g(x) \end{aligned} \tag{2.11}$$

Here $\epsilon g(x)$ represents the flux that crosses the edge of the jet, expressed as a function of x. Assuming now an expansion of the form:

$$\psi = \psi_o + \epsilon\psi_1 \tag{2.12}$$

and expanding $\psi(x,\epsilon t(x))$ in powers of ϵ, the following two problems for ψ_0 and ψ_1 can be

formulated:

$$\nabla^2\psi_o = 0$$
$$\psi_0(x,\infty) = \psi_\infty \tag{2.13}$$
$$\psi_0(x,0) = 0$$

and

$$\nabla^2\psi_1 = 0$$
$$\psi_1(x,\infty) = 0 \tag{2.14}$$
$$\epsilon\psi_1(x,0) = \epsilon g(x) - \epsilon t(x)\psi_{oy}(x,0)$$

If now we define the velocity profile of the jet to be given by

$$u = \frac{\partial\psi_o}{\partial y} + u_1\ F(x,y) \tag{2.15}$$

the right hand side of equation 2.14c represents, up to order ϵ, the flux involved in the second term of the velocity profile described by equation 2.15. Then an alternative way of writing equation 2.14c is:

$$\epsilon\frac{\partial\psi_1}{\partial x}(x,0) = \frac{\partial}{\partial x}\int_0^{\epsilon t(x)} u_1\ F(x,y)dy \tag{2.16}$$

If now, as done in reference 6, the excess velocity in the jet is represented by a Guasian exponential, equation 2.16 can be written:

$$\epsilon\frac{\partial\psi_1}{\partial x}(x,0) = \frac{\partial}{\partial x}\int_0^{\epsilon t(x)} u_1 \exp(-\alpha\frac{y^2}{b^2})\ dy \tag{2.17}$$

If $\frac{b}{\epsilon\ t(x)} << 1$, this equation becomes:

$$\epsilon\frac{\partial\psi_1}{\partial x}(x,0)\ \cong \sqrt{\frac{\pi}{4\alpha}}\frac{d}{dx}\ (u_1 b) \tag{2.18}$$

The boundary condition represented by this last equation can be restated in terms of a source distribution on the x axis of local intensity:

$$q_p(x) = -\sqrt{\frac{\pi}{\alpha}}\frac{d}{dx}(u_1 b) \tag{2.19}$$

Then the ψ_1 part of the solution consists of the flow field induced by the source distribution given by 2.19. In the case of the re augmentor, this will be the component of the field shown in figure 3b.

This flow field can also be computed with conformal mapping. Under transformation 2.6 the sink distribution given by 2.19 transforms into a distribution on the ξ axis. If dq_p is the differential sink strength at position ξ_o, the corresponding induced velocity in the z plane is:

$$dV_p = \frac{1}{2\pi}\frac{d\tilde{q}_p}{w(z) - \xi_o}\frac{dw}{dz} \tag{2.20}$$

with

$$d\tilde{q}_p = \tilde{q}(\xi_o)\frac{d\bar{x}}{d\xi}(\xi_o)\, d\xi_o \tag{2.21}$$

since

$$\frac{d\bar{x}}{d\xi} = \frac{1}{\pi}\left(1 - \frac{1}{\xi_o}\right) \tag{2.22}$$

the resulting velocity in the z plane is:

$$V_p = \frac{1}{2\pi}\frac{w}{w-1}\int_{\xi_j}^{\xi_1} \frac{\tilde{q}_p(\xi_o)\left(1 - \frac{1}{\xi_o}\right)}{w - \xi_o} d\xi_o \tag{2.23}$$

where ξ_j indicates the origin of the primary jet, and ξ_1 the end of the external region in the channel. These quantities can only take negative values. Hence the only singularity in 2.23 occurs at $\xi_o = w$. It is not possible to integrate 2.23 analytically. The integration can

be carried out numerically by discretizing $\tilde{q}_p$. Since $\tilde{q}_p$ depends on the inviscid solution, an iterative process is needed to solve for this discretization.

2.3.3 Flow field induced by the exhaust plume

This part of the analysis can be done along the same lines as the entrainment of the primary jet. However, the flow induced by the exhaust jet is not likely to affect the potential flow in the proximity of the inlet, which is the most important area as far as performance is concerned. Since the objectives of this study is performance evaluation, the exhaust field has not been included.

2.3.4 Viscous solution

The inner, viscous solution is obtained by applying an integral method to the time averaged flow quantities. A detailed description of the method is given in reference[6]. Making use of the boundary layer assumptions and neglecting the component of stress due to molecular viscosity, the equation of conservation of momentum in the x direction is:

$$\Gamma(u) = u\frac{\partial u}{\partial x} + \frac{\partial u}{\partial y}\int_o^y \frac{\partial u}{\partial x}d\xi + \frac{1}{\rho}\frac{dp}{dx} - \frac{1}{\rho}\frac{\partial \tau}{\partial y} = 0 \tag{2.24}$$

and the equation of conservation of mass:

$$\frac{\partial u}{\partial x} + \frac{\partial v}{\partial y} = 0 \tag{2.25}$$

To solve this equation a suitable representation for $u(x, y)$ valid from the primary nozzle exit to the exhaust nozzle exit plane is postulated in the manner shown in figure 4. Such a representation is of the form:

$$\hat{u}(x, y) = u_o(x) + u_1(x)\exp(-\alpha\frac{y^2}{b^2}) \tag{2.26}$$

In this equation $u_o(x), u_1(x)$ and $b(x)$ are unknown a priori. This representation also implies that the boundary layers on the inner side of the ejector walls are ignored[6]. The Reynolds stress τ is represented by a kinematic eddy viscosity model of the form:

$$\frac{\tau}{\rho} = \nu_t \frac{\partial \hat{u}}{\partial y} \tag{2.27}$$

where ν_t is assumed to scale in the following way:

$$\nu_t = k u_1 b \tag{2.28}$$

Here k is supposed to be a constant whose approximate value can be determined either by comparison with experimental results, or by requiring that the theory should reproduce already known results exactly. The requirement that the integral method should yield a rate growth of $\dot{b} = 0.1$ when applied to the two-dimensional turbulent free jet leads to a value of k of about 0.0283. Comparison between computed and measured inner flow fields in ejectors suggests that this value should be slightly larger. Values of k of up to 0.035 can be used without visible effects on the global aspects of performance, such as total mass flux and thrust augmentation. Substituting now 2.26 and 2.27 into 2.24 it is possible to obtain a system of n independent reduced equations by taking n moments of the operator $\Gamma(\hat{u})$ as follows:

$$\int_0^{h(x)} y^n \Gamma(\hat{u}) dy = 0 \tag{2.29}$$

Equations 2.29 plus conservation of mass constitute a set of four non-linear ordinary differential equations relating the functions u_o, u_1, b, p and their derivatives. In matrix form:

$$\begin{bmatrix} a_{11} & a_{12} & a_{13} & a_{14} \\ a_{21} & a_{22} & a_{23} & a_{24} \\ a_{31} & a_{32} & a_{33} & a_{34} \\ a_{41} & a_{42} & a_{43} & a_{44} \end{bmatrix} \begin{bmatrix} \dot{u}_o \\ \dot{u}_1 \\ \dot{b} \\ \dot{p} \end{bmatrix} = \begin{bmatrix} b_1 \\ b_2 \\ b_3 \\ b_4 \end{bmatrix} \tag{2.30}$$

In regions 1 and 2 this system reduces to a system of 2 equations for u_1 and b, since the matching conditions provide u_o and thus the pressure through the application of Bernoulli's

equation. Hence in regions where the outer flow is known the last two equations are disregarded and the system to be solved reduces to:

$$\begin{bmatrix} a_{12} & a_{13} \\ a_{22} & a_{23} \end{bmatrix} \begin{bmatrix} \dot{u}_1 \\ \dot{b}_1 \end{bmatrix} = \begin{bmatrix} b_1 & - & \dot{u}_o a_{11} & - & \dot{p} a_{14} \\ b_2 & - & \dot{u}_o a_{21} & - & \dot{p} a_{24} \end{bmatrix} \tag{2.31}$$

This two-equation system is only applied to region 1, while in region 2 the entrance and exit parameters are estimated by conservation considerations. In regions 3 and 4 the system is solved for all four variables.

2.3.5 Initial conditions for the inner solution

In this model the primary jet is idealized as a point source of momentum with no mass of its own, emerging from the so-called virtual origin. The location of the virtual origin is not known with certainty, and appears to be influenced by the conditions in which the experiment is conducted[8,9].

Absence of precise knowledge of the virtual origin amounts to an uncertainty in the present results which becomes less significant as the primary nozzle width decreases. In these calculations the virtual origin is assumed to coincide with the exit plane of the primary nozzle. The calculation is begun at a point slightly downstream of the virtual origin. The values of b and u_1 at this point are computed as if the primary jet had evolved as a free jet in still air, and by requiring that the momentum of this free jet be equal to do u_{oj}^2, where d_o is the primary nozzle width.

2.3.6 Viscous-inviscid matching

The matching is carried out in region 1 by setting

$$u_0(x) = v(x - \bar{x}_j, i0) \tag{2.32}$$

where $V = V_b + V_p$. Satisfaction of this equation would require an iterative procedure to compute V_p (2.3.2). A way to avoid this iteration, is to simply ignore the v_p component of inviscid flow. This would introduce a change in the augmentation ratio of the order of

2%. which justifies neglecting this contribution. In principle the matching process can be extended into region 2, however, the primary jet is fairly thick in this region. For this reason it is best to treat region 2 globally, without resolving the detailed velocity distribution. This is possible since, once the matching in region 1 is completed, the conditions at the beginning of region 2 become known, and the enforcement of mass and momentum conservation in integral form gives the conditions at the exit of region 2. This approach accounts for the viscous-inviscid interaction in region 2 in an indirect manner. From the end of region 2 on the calculation concerns itself with the viscous solution only.

2.3.7 Exit pressure matching

In addition to the viscous-inviscid matching, there is also a process leading to the matching of the exit pressure, which should equal the atmospheric pressure. This is done by considering the exit pressure as a function of the intensity of the momentum source, and using Newton's method to find the root of:

$$p_e(m_j) - p_{atm} = 0 \tag{2.33}$$

Hence,

$$m_j^{k+1} = \frac{m_j^k - p_e(m_j^k) - p_{atm}}{\frac{dp_e}{dm_j}(m_j^k)} \tag{2.34}$$

The derivatives in 2.34 can be approximated by finite differences and in most cases convergence is achieved within five cycles.

2.4 Augmentor of arbitrary shape

The generalization to augmentors of arbitrary shapes concerns the outer flow only. If the shape of two-dimensional augmentor deviates slightly from a straight channel, a perturbation analysis on the transformed plane can be carried out to compute the outer potential flow.

Consider an ejector shroud as shown in figure 5. The cowling can be seen as described by the functions $\epsilon f_1(x)$ and $\epsilon f_2(x)$ In the case that these functions take on values much smaller than unity, transformation 2.6 will map the cowling into the shape described by $\epsilon\tilde{f}(\xi)$, where $\epsilon \ll 1$. The fact that $\epsilon\tilde{f}(\xi)$ departs slightly from the axis allows for the linearization of the boundary conditions in the w plane, and this leads to simple integral form solutions for the perturbed velocity field. The perturbed problem would require the solution of integral equations if it were formulated in the physical plane directly. We will first look at the perturbed Borda component of the velocity field. Using again the concept of stream function, the boundary value problem in the upper half plane can be written:

$$\nabla^2\psi = 0 \tag{2.36a}$$

$$\frac{\partial\psi}{\partial\xi}(\xi,\epsilon\tilde{f}) = -\frac{\partial\psi}{\partial y}(\xi,\epsilon f)\epsilon\dot{\tilde{f}} \tag{2.36b}$$

$$\psi \to -\frac{u_b}{\pi}\tan^{-1}\frac{\eta}{\xi} \text{ at } \infty \tag{2.36c}$$

The condition at infinity reflects the sink at the origin of the transformed plane and assumes that the perturbation of the velocity field produced by the displacement $\epsilon\tilde{f}(\xi)$ vanishes at infinity. Transfering now the boundary conditions to the ξ axis we have:

$$\frac{\partial\psi}{\partial\xi}(\xi,o) + \epsilon\tilde{f}\frac{\partial^2\psi}{\partial\xi\partial y}(\xi,o) = \frac{-\partial\psi}{\partial y}(\xi,0)\epsilon\dot{\tilde{f}} + o(\epsilon^2) \tag{2.37}$$

Assuming the expansion $\psi = \psi_o + \epsilon\psi_1$, and substituting 2.35 we find the following problems for ψ_o, ψ_1:

$$\nabla^2\psi_o = 0 \tag{2.38a}$$

$$\frac{\partial\psi_o}{\partial\xi}(\xi,o) = 0 \tag{2.38b}$$

$$\psi_o \to -\frac{u_b}{\pi}\tan^{-1}\frac{\eta}{\xi} \text{ at } \infty \tag{2.38c}$$

and

$$\nabla^2\psi_1 = 0 \tag{2.39a}$$

$$\epsilon\tilde{f}\frac{\partial\psi_1}{\partial\xi}(\xi,o) = -\epsilon\dot{\tilde{f}}\frac{\partial\psi_o}{\partial y}(\xi,o) - \epsilon\tilde{f}\frac{\partial^2\psi_o}{\partial\xi\partial y}(\xi,o) \tag{2.39b}$$

$$\psi_1 \to \text{const} \quad \text{at } \infty \tag{2.39c}$$

The first problem yields the Borda mouthpiece solution for the straight channel case, hence

$$\psi_o = -\frac{u_b}{\pi}\tan^{-1}\frac{\eta}{\xi} \tag{2.40}$$

The second problem can be solved by looking at its boundary condition 2.38a, which after making use of 2.39 can be expressed:

$$\epsilon\tilde{f}\frac{\partial\psi_1}{\partial\xi}(\xi,0) = \dot{\tilde{f}}\ \frac{u_b}{\pi}\frac{1}{\xi} - \tilde{f}\ \frac{u_b}{\pi}\frac{1}{\xi^2} \tag{2.41}$$

Since $\frac{\partial\psi_1}{\partial\xi} = -v, \psi_1$ will correspond to the flow field produced by a source distribution on the ξ axis given by:

$$q = \frac{2u_b}{\pi}\left(\frac{\tilde{f}}{\xi^2} - \frac{\dot{\tilde{f}}}{\xi}\right) \tag{2.42}$$

Now it is necessary to express $\tilde{f}$ and $\dot{\tilde{f}}$ in terms of f and ξ. The real and imaginary parts of transformation 2.6 are

$$\pi y = \eta - \tan^{-1}\frac{\eta}{\xi} + \pi \tag{2.43}$$

$$\pi x = \xi - \ln\sqrt{\xi^2+\eta^2} - 1 \tag{2.44}$$

Focusing on equation 2.42, it is clear that for ξ of order 1,

$$\tan^{-1}\frac{\tilde{f}}{\xi} \cong \frac{\tilde{f}}{\xi} \tag{2.45}$$

For $\xi \to 0$, $\tilde{f} \to 0$ since all the points in the channel downstream at infinity map to the origin in the transformed plane. Substituting y by $1 - \epsilon f_i$ in 2.42, we have:

$$\frac{\tilde{f}}{\xi} = \tan(\pi\epsilon f_i + \tilde{f}) \tag{2.46}$$

where f_i takes the value of f_o for $\xi > 1$ and of f_1 for $\xi < 1$. As $x \to \infty$.

$$\frac{\tilde{f}}{\xi} \to \tan \pi\epsilon f_i \tag{2.47}$$

Since $\pi\epsilon f_i(x)$ is small for all values of x, 2.46 says that for $\xi \to 0$, 2.44 is also a good approximation. Assumption 2.44 is certainly safe for large ξ. If 2.46 is assumed to hold for any positive value of ξ, we find:

$$f(\xi) = -\frac{\pi\epsilon_i\xi}{\xi - 1} \tag{2.48}$$

Neglecting η^2 in 2.43 we find:

$$\frac{d(\pi x)}{d\xi} = 1 - \frac{1}{\xi} \tag{2.49}$$

From 2.47 and making use of 2.48 we get:

$$\dot{\tilde{f}} = -\epsilon\frac{df_i}{dx} - \epsilon\pi\frac{f_i}{\xi - 1} + \epsilon\pi\frac{f_i\xi}{(\xi - 1)^2} \tag{2.50}$$

With 2.49 and 2.47 the source intensity becomes:

$$q = \epsilon\frac{2u_b}{\pi}\left[\frac{1}{\xi}\frac{df_i}{dx} - \frac{\pi f_i}{(\xi - 1)^2}\right] \tag{2.51}$$

Hence the resulting perturbed Borda component of the velocity potential in the transformed plane will be expressed as:

$$\phi_b = -\frac{u_b}{\pi}\ln w + \frac{1}{2\pi}\int_0^\infty q(\xi_0)\ln(w - \xi_0)d\xi_0 \tag{2.52}$$

and, after substitution of $q(\xi_o)$ by its expression 2.50, the corresponding complex velocity in the physical plane is given by:

$$V_b + \Delta V_b = -\frac{u_b}{w-1} - \epsilon u_b \frac{w}{w-1}\left[\frac{1}{\pi}\int_0^\infty \frac{\dot{f}_i}{\xi_0(\xi_0 - w)} d\xi_0 \right.$$

$$\left. - \int_0^\infty \frac{f_i}{(\xi_0 - 1)^2(\xi_0 - w)} d\xi_0 \right]. \tag{2.53}$$

2.4.1 Convergence conditions

Requirements for the existence of the integrals in 2.52 need to be specified. To this end the behavior of $\epsilon\tilde{f}$ near $\xi = 0$ and $\xi = 1$ will be investigated.

For small ξ, equation 2.43 can be written:

$$\pi x = -\ln\sqrt{\xi^2 + \eta^2} \tag{2.54}$$

replacing $\tilde{f}$ with η in 2.46 we have that

$$\eta \sim \pi\epsilon f_i \xi \quad \text{as } \xi \to \infty \tag{2.55}$$

substituting in 2.53 we find, for $\xi \to 0$ and $x \to \infty$

$$\xi \sim e^{-\pi x} \tag{2.56}$$

This means that the slope of the inner side of the shroud should vanish at least like $e^{-\pi x}$ at infinity in order for the first integral in 2.52 to converge. This is not a restriction, since $f = 0$ beyond the nozzle exit plane. Now we analyze the behaviour of f_i close to $\xi = 1$, to do so, y is replaced by $1 - \epsilon f_i$ in 2.42 to obtain:

$$\xi = \frac{1}{1 + \frac{\pi\epsilon f_1}{\eta}} \tag{2.57}$$

In the proximity of $\xi = 1$, $\frac{\pi\epsilon f_i}{\eta} \ll 1$, expanding 2.56 one finds:

$$\xi \cong 1 - \frac{\pi\epsilon f_1}{\eta} + O\left(\frac{\pi\epsilon f_i}{\eta}\right)^2 \tag{2.58}$$

and

$$\pi\epsilon f_i = \eta(1-\xi) + O\left[\frac{(\pi\epsilon f_i)^2}{\eta}\right] \quad \text{as } \xi \to 1 \tag{2.59}$$

To relate η to ξ for $\xi \to 1$, consider an expansion of ϵf_i about $x = 0$ in the form

$$\epsilon f_i(x) \sim \delta x \tag{2.60}$$

Between 2.58, 2.42 and 2.43 we find

$$\frac{1}{\delta}\left(-\eta + \tan^{-1}\frac{\eta}{\xi}\right) = \xi - \ln\sqrt{\xi^2+\eta^2} - 1 \tag{2.61}$$

Defining now

$$\Delta = 1 - \xi, \tag{2.62}$$

replacing 2.61 into 2.60 and expanding both sides we find:

$$\eta^2 + \frac{2\Delta}{\delta}\eta - \Delta^2 = O(\eta\Delta^2) + O(\eta^3) \tag{2.63}$$

Neglecting the higher order terms on the right hand side, equation 2.62 can be solved for η:

$$\eta = \frac{\Delta}{\delta}\left(-1 \pm \sqrt{1+\delta^2}\,\right) \tag{2.64}$$

since for $\Delta > 0$, $\eta > 0$ the right sign in the square root in 2.63 is positive, then:

$$\eta \sim (1-\xi)\frac{1}{\delta}\left[\sqrt{1+\delta^2} - 1\right] \tag{2.65}$$

substituting 2.64 in 2.58 we find that:

$$\epsilon f \sim (1-\xi)^2 \frac{1}{\pi\delta}\left[\sqrt{1+\delta^2}-1\right] \quad \text{as } \xi \to 1 \tag{2.66}$$

This implies that the second integral in 2.52 also exists, since the singularity at $\xi = 1$ is cancelled out. It is important to recognize that this conclusion depends on assumption 2.59, which presuposes a cusped shroud leading edge. Since one is interested in the flow field at some distance from the leading edge, and since this conclusion is not limited to small δ, this assumption does not constitute a restriction in practical cases.

2.4.2 Resulting outer potential flow field

The resulting outer field will contain, in addition to the perturbed Borda component, the flows induced by entrainment into the primary and the exhaust plume. In a strict sense the flow due to entrainment should be computed on the basis of the perturbed cowling shape. However, the difference between entrainment fields resulting from a calculation based on the perturbed cowling shape and another one based on the straight-walled cowling shape can be neglected in this approximation. With this in mind, and leaving out the influence of the entrainment by the exhaust, the resulting outer flow in the physical plane is given by:

$$\phi = \phi_b + \Delta\phi_b + \phi_p \tag{2.67}$$

2.4.3 Thrust augmentation

Thrust augmentation is usually defined as the ratio of the thrust produced by the augmentor to the thrust that would be produced by the primary jet discharging adiabatically, in isolation and in an environmnent at atmospheric pressure. The computation of the thrust augmentation in our case is simplified by the fact the flow is incompressible. The shroud will produce thrust due to the integrated effect of the presure acting on its surface. The computation of the resulting force on the shroud will be carried out first

on an augmentor with parallel, infinitely thin walls. In this case all the forces acting on the shroud are concentrated at the leading edge as a result of infinite suction acting on an infinitesimal area. To compute this force we apply Blassius theorem to the indented contour γ sketched in figure 6. Neglecting the effect of entrainment into the exhaust jet, the force acting in the leading edge will be given by:

$$F = \frac{1}{2} i \oint_{\delta} \left(\frac{d\phi_b}{dz} + \frac{d\phi_p}{dz} \right)^2 dz \tag{2.68}$$

This equation contains the Borda component of the external flow and the flow induced by the primary jet entrainment. It cannot be evaluated exactly because ϕ_p is not known analytically. An approximate solution for equation 1 would require to provide an approximation for q_p, however it is possible to show that the effect of ϕ_p on φ is usually not important. To estimate this effect, lets represent the primary jet entrainment by a single sink located at the virtual origin, of strength $\bar{q}_p$, where $\bar{q}_p$ is the entrainment into the primary jet between the origin and the inlet plane. Then we have:

$$\tilde{\phi}(w) = -\frac{u_b}{\pi} \ln w + \frac{\bar{q}_p}{2\pi} \ln(w - \xi_j) \tag{2.69}$$

Since in the neighborhood of the leading edge the velocity induced by entrainment is significantly smaller than the Borda component of the potential flow, equation 2.67 can be approximated by:

$$F \sim \frac{1}{2} \, i \oint_{\delta} \left[\frac{u_b^2}{\pi} \frac{1}{(w-1)^2} - u_b \bar{q}_p \frac{w}{(w-1)^2 (w - \xi_j)} \right] dz \tag{2.70}$$

In the proximity of $z = i$ we get

$$w \cong 1 + \sqrt{2\pi(z - i)} \tag{2.71}$$

Substituting in equation 2.69 and carrying out the integration we find

$$T \sim u_b^2 + \frac{u_b \bar{q}_p}{1 - \xi_j} \tag{2.72}$$

where T is equal to $2F$. Notice that F is real, which indicates the suction force acts parallel to the x axis.

The augmentation ratio is given by:

$$\varphi = 1 + \frac{T}{mj} \tag{2.73}$$

Defining now the parameter K[6]

$$K = \frac{2u_b^2}{m_j} \tag{2.74}$$

and approximating $\bar{q}_p$ by the product u_1, b taken at the inlet plane,

$$\varphi = 1 + \frac{K}{2}\left(1 + \frac{(u_1 b)_{inlet}}{1 - \xi_j}\right) \tag{2.75}$$

In practical cases the term containing $(u_1 b)_{inlet}$ is of order 0.2, which indicates that the effect on φ due to primary jet entrainment is fairly small.

In the case of a shroud of arbitrary shape, the computation of leading edge suction force cannot be achieved using Blasius theorem because the potential $\Delta\phi_b$ is known only approximately, and singular behavior in such cases is known to lead to wrong values of suction forces[10]. Nevertheless it can be argued that equation 2.71 is also valid in the general case. The first term in the right hand side of 2.71 can be interpreted as the momentum flux infinitely far downstream in the two-dimensional channel used to get the basic outer solution. As seen in figure 6, the general case can be treated by assuming that sufficiently far downstream the inner flow develops in a channel coincident with the basic parallel-wall channel. Hence the momentum flux infinitely far downstream will be identical in both cases. If the shroud has a diffuser with projected vertical area Ω, and defining the non-dimensional pressure[6] $\bar{p} = \frac{2p}{\rho u_b^2}$, the net thrust augmentation becomes:

$$\varphi = 1 + \frac{K}{2}(1 + \int p d\Omega) \tag{2.75}$$

where the contribution due to the primary jet entrainment has been left out.

3. RESULTS AND CONCLUSIONS

3.1 Wedge-shaped augmentor

An ejector shape of practical significance is shown in figure 7. The shroud is characterized by a wedge-like inlet of angle δ extending to the distance x^*. The main mixing part of the channel has parallel walls and the diffuser has arbitrary shape. The study of this problem is important in that it will provide an understanding of some of the effects of inlet shape on the performance. The analysis done here will reveal to what extent a divergent inlet affects performance through the viscous-inviscid interaction with the primary jet. In this particular case the terms in equation 2.52 can be evaluated analytically. In order to do so, expressions for f_i and f_i have to be found in the transformed plane.

We have; for small δ:

$$\epsilon f_i(x) \cong \delta x; \; x < x^* \tag{3.1a}$$

$$\epsilon f_i(x) \cong \delta x^*; \; x > x^* \tag{3.1b}$$

Now identifying η with $\tilde{f}(\xi)$ in equation 2.47 and then substituting in equation 2.43 we get:

$$\pi x = \xi - \ln \xi - \ln \sqrt{1 - \frac{\pi^2 \epsilon^2 f_i}{(\xi - 1)^2}} - 1 \tag{3.2}$$

With the assumption that $\epsilon f_i \ll 1$ everywhere,

$$\frac{\pi^2 \epsilon^2 f_1}{(\xi - 1)^2} \ll 1 \quad \text{for } \xi \ll 1 \tag{3.3}$$

Since, according to 2.65, $\epsilon f_i \sim (1 - \xi)^2 \delta$ for small δ and $\xi \to 1$.

$$\frac{\pi^2 \epsilon^2 f_i}{(\xi - 1)^2} \ll 1 \quad \text{for } \xi \to 1 \tag{3.4}$$

Hence the logarithm in 3.2 can be linearized in the range 0 to 1, and the following guadratic equation for $\pi\epsilon f_i$ is found:

$$\pi^2\epsilon^2 f_i^2 \frac{1}{2(\xi-1)^2} + \frac{\pi\epsilon f_i}{\delta} + 1 - \xi + \ln\xi = 0 \tag{3.5}$$

solving for $\pi\epsilon f_i$:

$$\pi\epsilon f_i = \frac{(\xi-1)^2}{\delta}\left[-1 + \sqrt{1 - 2\delta^2\frac{(1-\xi+\ln\xi)}{(\xi-1)^2}}\right] \tag{4.6}$$

The positive sign in the square root is required to obtain positive $\pi\epsilon f_i$ for $\xi \to 1$. If now expression 3.1 and 3.6 are substituted in 2.52 we get:

$$V_b + \Delta V_b = u_b\frac{1}{w-1} - u_b\frac{w}{w-1}\left[\frac{\delta}{\pi}\int_\xi^1 \frac{d\xi_o}{\xi_o(\xi_o-\xi)} - \delta x^*\int_o^{\xi^*}\frac{d\xi_o}{(\xi_o-1)^2(\xi_o-\xi)}\right.$$

$$\left. + \frac{1}{\delta\pi}\int_{\xi^*}^1 \frac{1-\sqrt{1-2\delta^2(1-\xi_o+\ln\xi_o)/(\xi_o-1)^2}}{\xi_o-\xi}d\xi_o\right] \tag{4.7}$$

Carring out these integrations and expanding the integrand of the last integral for small δ we find:

$$V_b + \Delta V_b = -u_b\frac{1}{w-1} - \delta u_b\frac{w}{w-1}\left[\frac{1}{\pi w}\ln\frac{\xi^*(1-w)}{\xi^*-w}\right.$$

$$- x^*\left[\frac{\xi^*}{(w-1)(\xi^*-1)} + \frac{1}{(w-1)^2}\ln\frac{\xi^*-w}{w(\xi^*-1)}\right]$$

$$\left. + \frac{1}{\pi}\int_{\xi^1}^{\xi^*}\frac{1-\xi_o+\ln\xi_o}{(\xi_o-1)^2(\xi_o-w)}d\xi_o\right] \tag{4.8}$$

This equation gives an algebraic expression for the perturbed outer field. It can also be seen as a first order expansion in powers of δ. It is important to notice that the expansion of the square root in the last integral of equation 4.7 requires, due to the logarithm in the numerator that x^* should be about unity. If this were not the case, the full integral

as in 4.7 should be used. In the case discussed next $x^* = 1$. Figure 7 shows the thrust augmentation as a function of the wedge angle. We see that there is essentially no change of the performance for different angles. This result suggests that the particular details of the inlet shape don't have a first order effect on the thrust augmentation.

3.2 Straight-walled augmentors

The theory is now applied to an augmentor with a shroud consisting of two thick flat plates, as shown in figure 8, and the results are compared with the experimental findings reported in reference 5. Although such ejectors have thick walls, the results of the previous section suggest that the walls could be idealized as thin flat plates. This was done to obtain the results shown below.

Figure 9 shows the calculated and computed velocity distributions in the inner flow for the ejectore sketched in figure 8, taken at the shroud inlet and exit stations. Here the horizontal component of velocity is presented in dimensional form; this is done by rescaling the computed non-dimensional velocity in a way that m_j becomes identical to the measured primary nozzle thrust. The computations were carried out with two different values of the eddy viscocity scaling factor k. Values of k larger than 0.0283 seem appropriate. Although there is a visible change in the velocity distribution between the two cases, global quantities such as thrust augmentation are practically the same. This indicates that, within limits, the choice of k is not critical. Figure 10 shows the effect of the position of the primary nozzle on performance for the same augmentor. We see that, in the absence of separation, the optimum position of the primary nozzle seems to be close to the inlet plane. The agreement with experiments appears to be extremely good in this particular case. Figure 11 shows computations for an augmentor obtained by attaching a diffuser to the one shown in figure 8, also reported in reference 5. Dependence of performance on diffuser angle is shown, where the negative contribution of the pressure acting on the vertical projection of the diffuser area is indicated by the spacing between the augmentation curve and its leading edge suction component. We see that this detrimental effect becomes

more pronounced at large diffusion angles, but in none of the computed cases appears to offset the positive contribution to augmentation, as a result of which the augmentation ratio increases monotonically with area ratio. The predicted value falls within 8% of the measurements.

In figure 12 the diffuser area ratio was kept constant as the length of the diffuser was varied. We see that under this conditions the performance changes very little. This result would indicate that the design of the diffuser could be based on boundary layer separation criteria only.

The effect of overall length to width ratio of the augmentor, for varying diffuser angles, is illustrated in figure 13. In these computation the efficiency of the diffuser appears to be weakly dependent on augmentor length.

3.3 Conclusions

A methodology for the calculation of two-dimensional ejector performance has been developed, which, combining analytical and integral methods, allows for a fast and economical computation. Typical computation times are of the order of two to five seconds on an IBM 3081 processor. The most important limitation in the internal flow treatment is given by the modelling of the Reynolds stress. Although the eddy viscocity model used here appears satisfactory for global estimations, further improvement, particularly in the local quantities of the flow field should result from upgrading the stress model. Predicted performance falls within ten percent of measured values and can be considered reasonable.

Regarding augmentor performance, the main observations are:

1. In the absence of separation, the particulars of the inlet do not have a first order effect on performance.
2. The optimum position for the primary nozzle lies close to the inlet plane.
3. Considerable changes in the scaling factor k for the eddy viscocity are felt much more strongly in the local velocity distribution in the inner viscous flow than in performance.
4. For a fixed overall augmentor length and fixed diffuser area ratio, diffuser length does

not have a significant effect on performance.

5. As the diffuser area ratio increases, the augmentation appears to increase monotonically.
6. The efficiency of the diffuser $\frac{\partial \varphi}{\partial \beta}$, depends very weakly on the overall length of the augmentor.

Further research in this area will focus on improved modeling of the outer flow and matching process, improved Reynolds stress description and on an inner flow formulation that accounts for compressibility and temperature effects.

REFERENCES

1. K. E. Hickman, P. G. Hill and G. B. Gilbert, "Analysis and testing of high entrainment single-nozzle jet pumps with variable area mixing tubes", NASA CR 2067, 1972.
2. G. B. Gilbert and P. G. Hill "Analysis and testing of two-dimensional slot nozzle ejectors with variable area mixing sections", NASA CR 2251, 1973.
3. P. M. Bevilaqua and A. D. DeJoode "Viscid/inviscid interaction analysis of thrust augmenting ejectors", Workshop on Thrust Augmenting Ejectors, NASA CP 2093, 1979.
4. P. M. Bevilaqua, C. J. Woan and E. F. Shum, "Viscid/inviscid interaction analysis of ejector wings", Ejector Workshop for Aerospace Applications, AFWAL-TR-82-3059, 1982.
5. L. Bernal and V. Sarohia, "Entrainment and mixing in thrust augmenting ejectors", AIAA paper no. 83-0172, 1983.
6. D. Tavella and L. Roberts, "Analysis of confined turbulent jets", JIAA TR 51, Stanford University, 1982.
7. P. G. Hill, "Turbulent jets in ducted streams", JFM, 22, Part 1, 1965.
8. N. E. Kotsovinos, "A note on the spreading rate and virtual origin of a plane turbulent jet", JFM, Vol 77, Part 2, 1976.
9. P. Bradshaw, "Effect of external disturbances on the spreading rate of a plane turbulent jet", JFM, Vol. 80, Part 4, 1977.
10. M. VanDyke, "Perturbation methods in fluid mechanics", Parabolic Press, Palo Alto, CA, 1975.

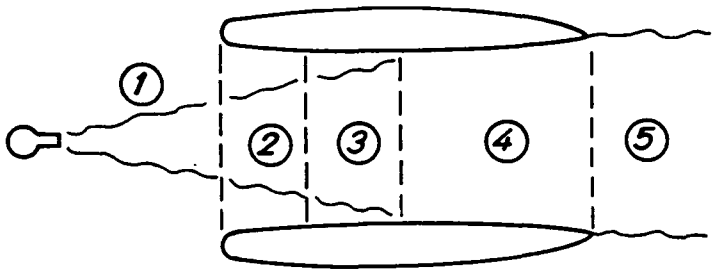

Figure 1. Flow regions

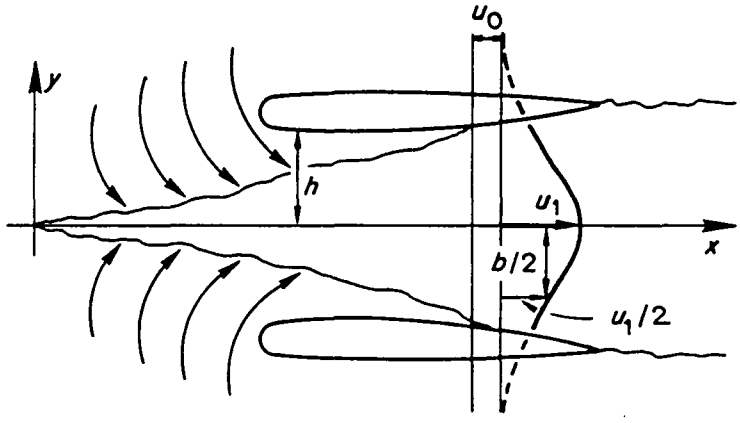

Figure 2. Inviscid and viscous flow fields

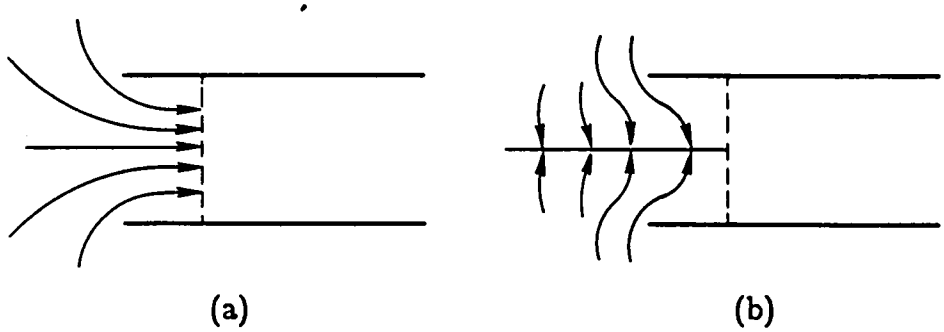

Figure 3. Components of inviscid flow field

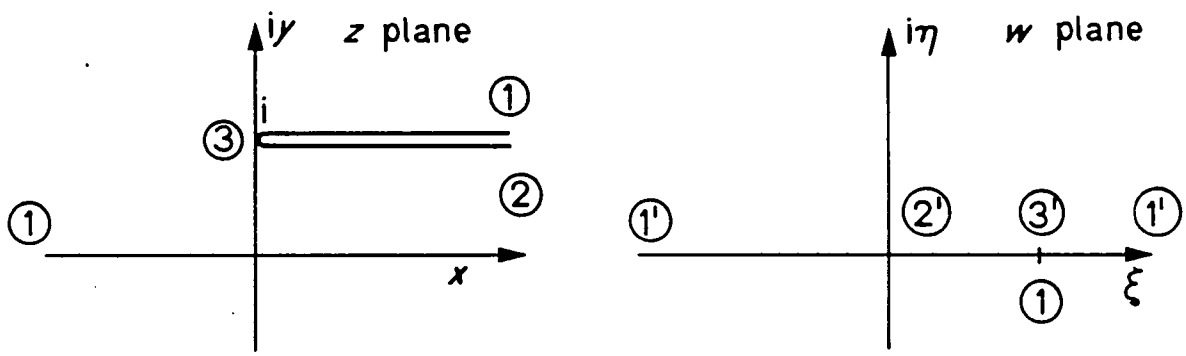

Figure 4. Mapping of outer field

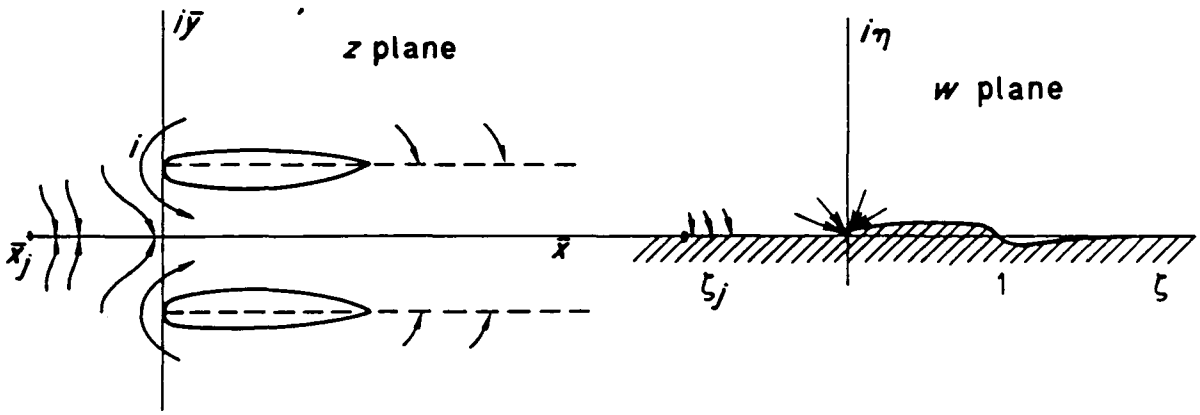

Figure 5. Augmentor of arbitrary shape

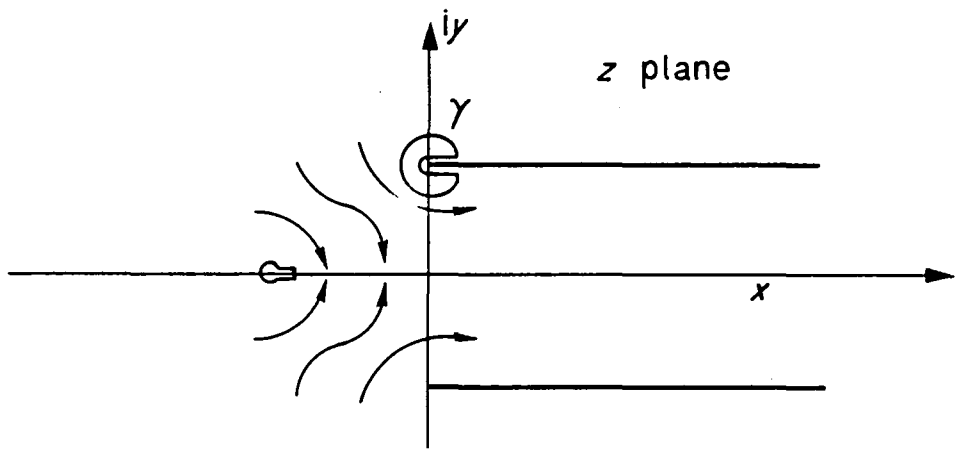

Figure 6. Computing leading edge thrust

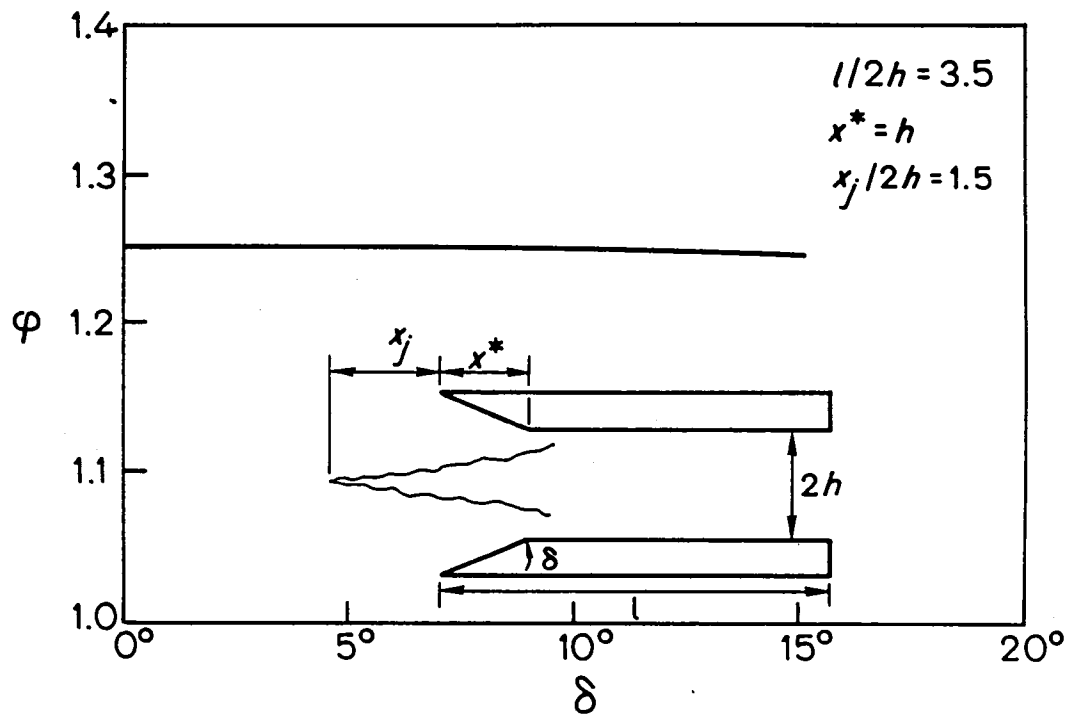

Figure 7. Augmentor with wedge-shaped inlet

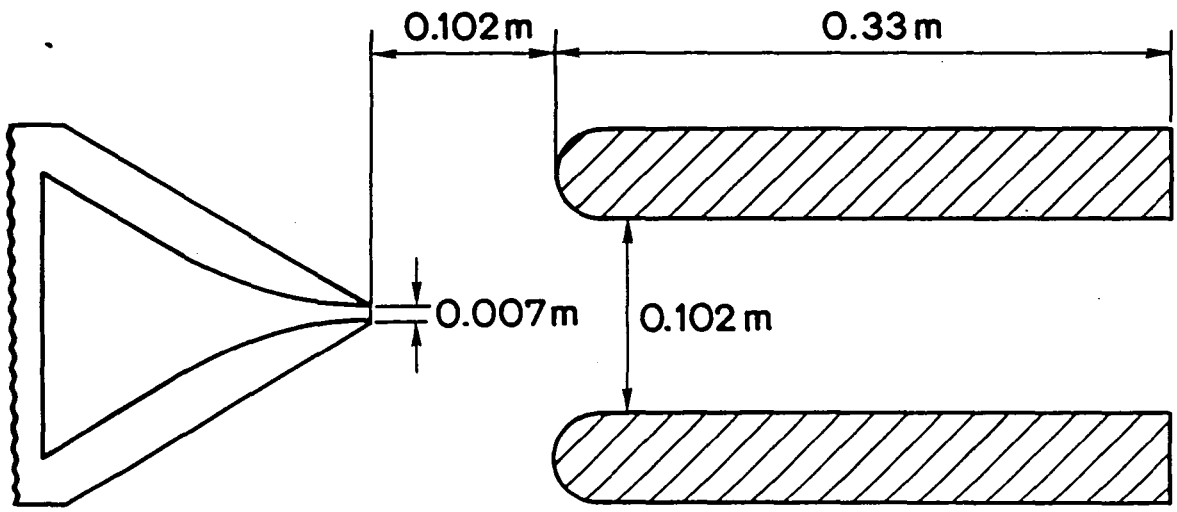

Figure 8. Augmentor tested at J.P.L.[5]

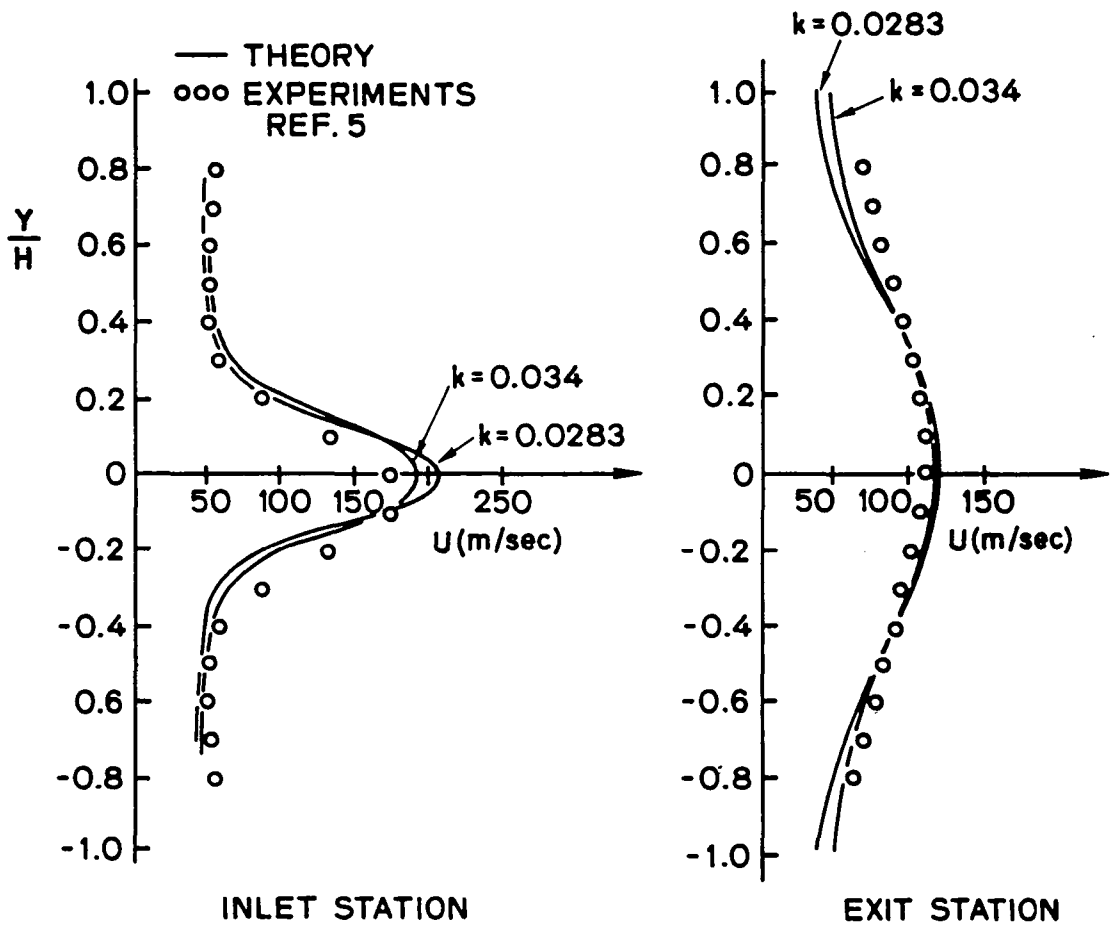

Figure 9. Viscous solution for J.P.L. augmentor

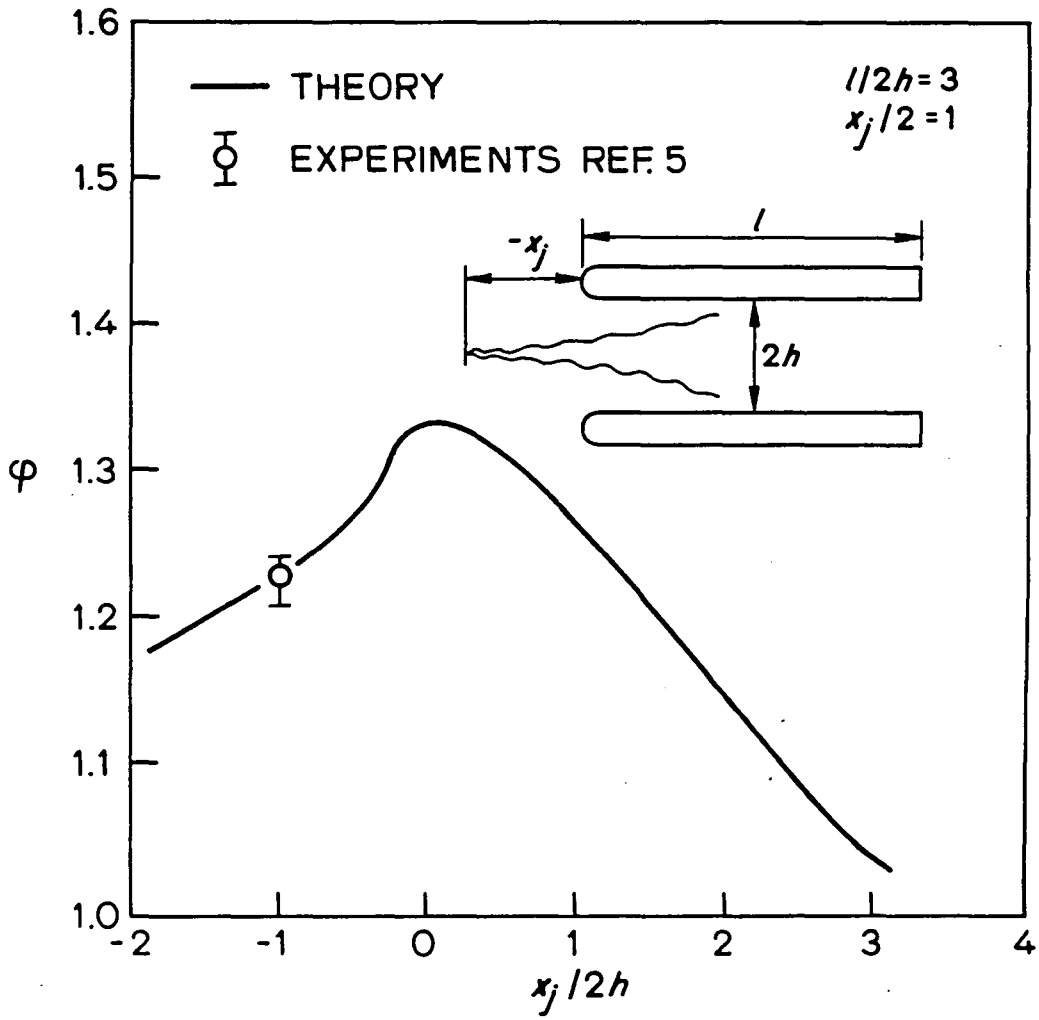

Figure 10. Effect of primary nozzle position

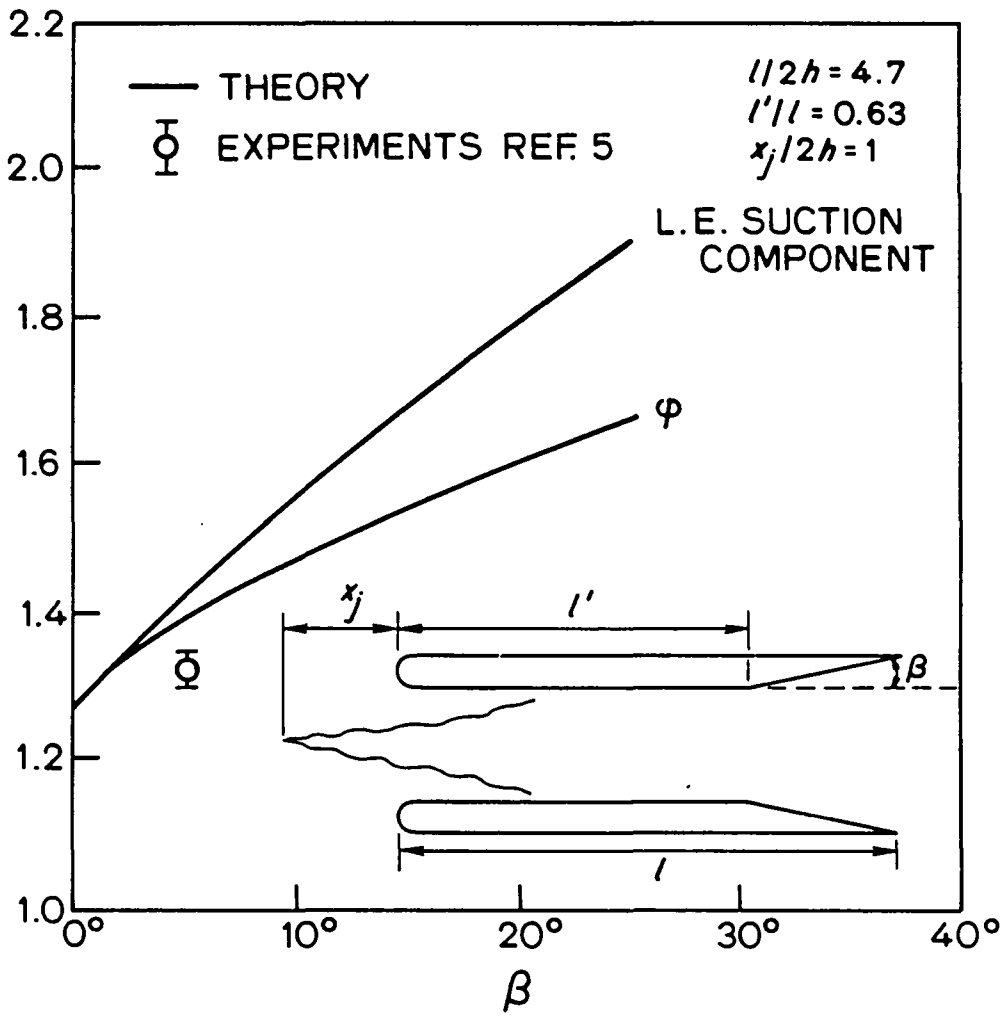

Figure 11. Effect of diffuser angle

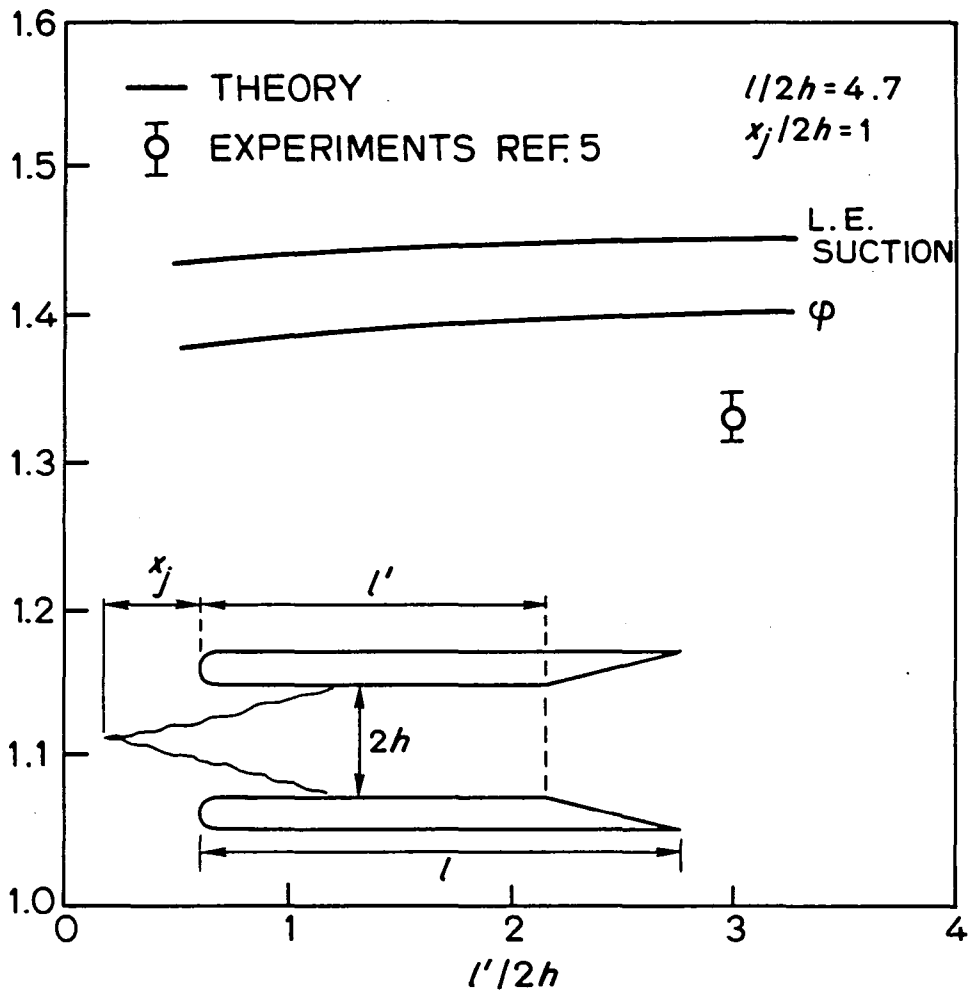

Figure 12. Effect of diffuser length

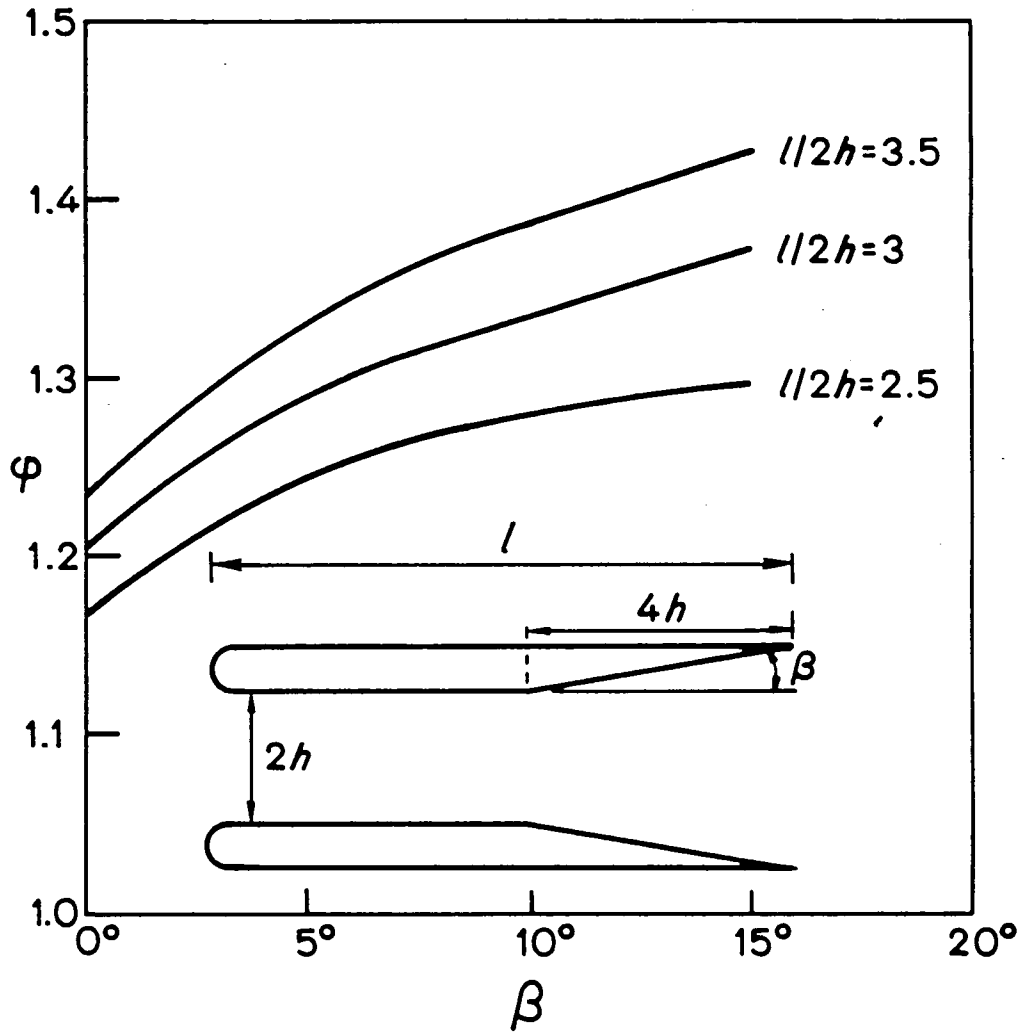

Figure 13. Effect of overall length

End of Document